Bio-Design and Manufacturing (2024) 7:43–56
https://doi.org/10.1007/s42242-023-00258-y

RESEARCH ARTICLE

Transfer film effects induced by 3D-printed polyether-ether-ketone with excellent tribological properties for joint prosthesis

Yang Li[1,2] · Jibao Zheng[1,2] · Changning Sun[1,2] · Dichen Li[1,2]

Received: 14 March 2023 / Accepted: 11 August 2023 / Published online: 28 November 2023

Abstract

Based on the building principle of additive manufacturing, printing orientation mainly determines the tribological properties of joint prostheses. In this study, we created a polyether-ether-ketone (PEEK) joint prosthesis using fused filament fabrication and investigated the effects of printing orientation on its tribological properties using a pin-on-plate tribometer in 25% newborn calf serum. An ultrahigh molecular weight polyethylene transfer film is formed on the surface of PEEK due to the mechanical capture of wear debris by the 3D-printed groove morphology, which is significantly impacted by the printing orientation of PEEK. When the printing orientation was parallel to the sliding direction of friction, the number and size of the transfer film increased due to higher steady stress. This transfer film protected the matrix and reduced the friction coefficient and wear rate of friction pairs by 39.13% and 74.33%, respectively. Furthermore, our findings provide a novel perspective regarding the role of printing orientation in designing knee prostheses, facilitating its practical applications.

✉ Dichen Li
dcli@mail.xjtu.edu.cn

1 State Key Laboratory for Manufacturing System Engineering, School of Mechanical Engineering, Xi'an Jiaotong University, Xi'an 710054, China

2 National Medical Products Administration (NMPA) Key Laboratory for Research and Evaluation of Additive Manufacturing Medical Devices, Xi'an Jiaotong University, Xi'an 710054, China

Graphic abstract

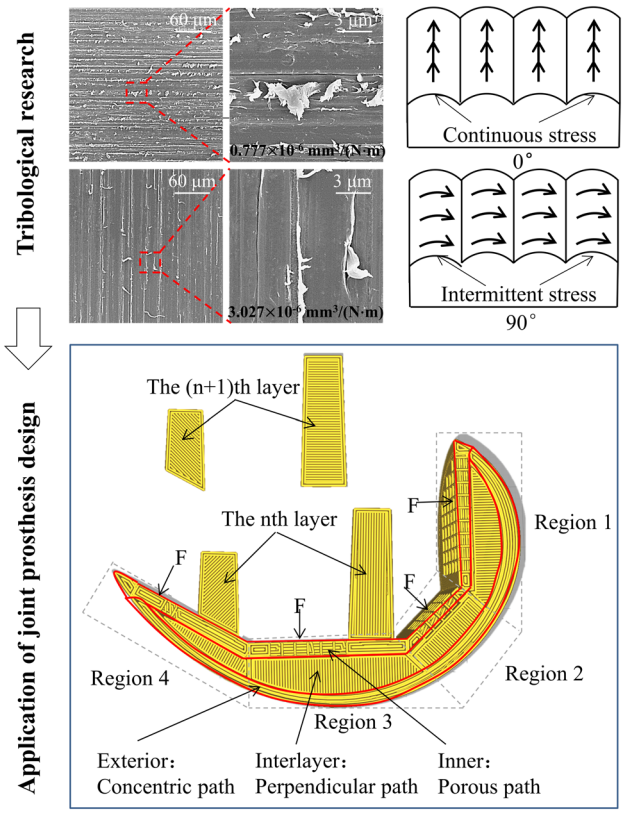

Keywords 3D printing orientation · Transfer film · Tribological properties · Polyether-ether-ketone · Knee prosthesis

Introduction

Artificial joint prostheses, an established strategy to replace damaged joints, can effectively provide mobility and comfort to patients suffering from severe joint diseases [1–3]. Currently, metal joint prostheses are widely used to fabricate various joints in the human body, such as titanium (Ti) alloy hip and cobalt chromium molybdenum (CoCrMo) alloy knee joints [4, 5]. However, recent developments have gradually shifted toward polymer joints, especially polyether-ether-ketone (PEEK) prostheses [6–8]. PEEK is highly regarded for its favorable biocompatibility and impressive mechanical properties comparable to natural cortical bone strength [9–14]. Notably, PEEK has outstanding wear resistance and lower density than metallic materials [15–19], making it a highly promising material for artificial joints.

Several reports have investigated the tribological properties of PEEK [20–23]. For instance, Cowie et al. employed injection molding to fabricate PEEK plates and ultrahigh molecular weight polyethylene (UHMWPE) pins and investigated their wear performance [24]. The results demonstrated that UHMWPE against PEEK exhibited a wear rate equivalent to that of UHMWPE against CoCrMo alloy. Zhang et al. compared the size distribution of wear debris of PEEK and CoCrMo alloy pins against UHMWPE plates, respectively [25]. Their findings indicated that the wear debris from CoCrMo against UHMWPE larger than 30 μm accounted for 0.83%, while the wear debris did not exceed 30 μm from PEEK against UHMWPE. Wear particles can trigger the release of bone resorption factors from macrophages, causing osteolysis. The smaller the volume of wear particles, the lower the risk of osteolysis [26–28]. However, the PEEK joint prosthesis specimens fabricated using the traditional injection molding process are limited to homogeneous structures and materials with a single function, making them unsuitable to meet the clinical needs of multifunctional joint prostheses.

Additive manufacturing, also referred to as three-dimensional (3D) printing, is an innovative technique for constructing products by accumulating materials layer by layer. Among various 3D printing methods, fused filament fabrication (FFF) can control the distribution of materials in a 3D space by regulating the real-time powder feeding

amount, thus enabling the product to have different functions in different regions [29–33]. The building principle of FFF determines that the printed surface is composed of aligned filaments, which can form a "groove" that imparts texture with high-stress "hills" and low-stress "valleys." When the sliding direction of friction is along the different printing orientations of filaments, the distribution of stress might vary due to the groove texture, which significantly affects the tribological properties. Although studies have explored the influence of printing orientation on the tribological properties of polylactic acid (PLA) against steel [34, 35], as the mechanical properties of PLA are significantly lower than those of PEEK, they are unsuitable for clinical prostheses. Besides, as steel is considered inappropriate for use in joint prostheses, further research should be performed using UHMWPE. Consequently, studying the effects of printing orientation on the tribological properties of PEEK is particularly important for supporting clinical applications.

In this study, we fabricated PEEK pins with different printing orientations through FFF 3D printing and investigated the effects of printing orientation on their tribological properties. We evaluated the friction coefficient, wear volume, and wear rate using pin-on-plate experiments, characterized the wear morphologies using microstructure analysis, and measured the corresponding surface roughness and wear depth. We also discussed how transfer films are formed in different orientations. Using printing orientation in the design of knee prosthesis as an example, we demonstrated the practical application of our findings.

Materials and methods

Materials

The PEEK (1.3 g/cm^3) powder (Victrex Co., Ltd., UK), with a particle diameter of 50 μm, was dried in a drying cabinet at 100 °C for 4 h and then fed into a twin-screw extruder (YTG-25, Yongtuo Technology Co., Ltd., China) to obtain the PEEK filaments with uniform diameters of 1.75 mm. The UHMWPE (0.945 g/cm^3) plates (Suzhou Microport Joint Medical Co., China) were cut into 20 mm×20 mm×5 mm (length × width × thickness) rectangles with a surface roughness of Ra<0.5 μm. Newborn calf serum solution (Wisent Biotechnology Co., Ltd., Canada) was diluted to a protein content of 20 g/L with deionized water, according to ISO 14243-1:2009.

Fabrication of PEEK pins and tribological tests

Figures 1a and 1b show the fabrication and post-treatment of PEEK pins with different printing orientations. The PEEK pins (diameter 5 mm, length 18 mm) were fabricated using an FFF 3D printer (Engineer 250, Jugao Additive Intelligent Manufacturing Technology Development Co., Ltd., China) with a nozzle diameter of 0.4 mm, layer thickness of 0.2 mm, printing temperature of 420 °C, and printing speed of 20 mm/s. The exterior and interior of the PEEK pins were sliced into concentric and perpendicular paths, respectively, in the slicing model. The same specimens were fabricated with the 3D printing process and then twisted relative to the sliding direction to form 0°, 22.5°, 45°, 67.5°, and 90° friction pairs in the tests. After printing, the PEEK pins were polished to a surface roughness of Ra<1.5 μm and annealed at a constant temperature of 200 °C for 30 min to improve crystallinity.

The tribological experiments were implemented using a pin-on-plate tribometer (UMT-2, Center of Trobology Friction and Wear Testing Machine Co., Ltd., USA) (Fig. 1c). The PEEK pins and UHMWPE plates were immersed in newborn calf serum medium to wear in the reciprocation model with the following wear parameters: reciprocating stroke of 6 mm, frequency of 1 Hz, applied load of 40 N (2 MPa), and test number of 10,000 times. In the control group, no reciprocating PEEK and UHMWPE specimens were immersed in the lubricating medium to avoid errors generated by the water absorption of the specimens. Each group was conducted in three replicates at room temperature (n=3). Before the tests, the PEEK pins and UHMWPE plates were ultrasonically cleaned with detergent and deionized water for 10 min, respectively. Then, they were dried in a vacuum drying cabinet at 50 °C for 8 h and weighed alternately by a scale with a resolution of 0.001 mg. These procedures were repeated once again after the wear tests. The real-time and average friction coefficient curves were recorded using a tribometer. The wear volume and wear rates were calculated according to the mass change of the friction pair before and after wear.

Characterization

The wear surface morphologies of PEEK were observed by scanning electron microscopy (SEM, su-8010, Hitachi, Japan) at an acceleration voltage of 10 kV, while those of UHMWPE were characterized by laser scanning confocal microscope (OLS4000, Lext, Japan). The relevant surface roughness (Ra), wear depth, and wear width (the distance between two ridge peaks, i.e., the distance from the nearest local peaks on either side of a furrow) on the surface of UHMWPE were also calculated. Three samples were measured in each condition, and five uniformly distributed furrows were measured in each sample. The composition of the transfer film formed on the surface of PEEK was analyzed by Fourier transform infrared spectroscopy (FTIR, Nicolet iS10, Thermo Fisher, USA) within the range of 500–4000 cm^{-1} and X-ray diffractometer (XRD, Advanced D8 A25, Brook, Germany) at a scanning rate of 8 °/min

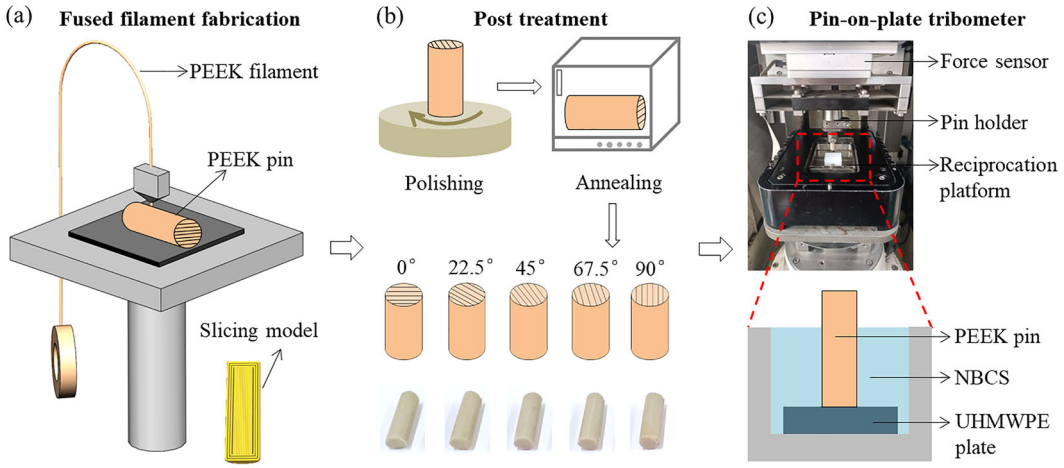

Fig. 1 PEEK pins with different orientations during **a** fabrication and **b** post-treatment. **c** Schematic diagram of the pin-on-plate tribometer. PEEK: polyether-ether-ketone; UHMWPE: ultrahigh molecular weight polyethylene; NBCS: newborn calf serum

from 10° to 50° of scattering angles. The area of the transfer film and its ratio on the matrix were counted using ImageJ. X-ray photoelectron spectroscopy (XPS, Thermo Fisher ESCALAB Xi+ , Thermo Fisher, USA) was equipped with an X-ray lamp with the Al Kα (1486.6 eV) anode to irradiate the specimen surface. After calibrating the C1s peak to 284.8 eV, peak fitting was performed using the Avantage software.

Finite element (FE) analysis

The FE models of the knee joint at −30°, 0°, 45°, and 90° flexion angles were constructed using the ANSYS software to analyze the biomechanics of the knee prosthesis. The mesh element of the models was SOLID187. The mesh size of the contact region between the femoral condyle and tibial tray was 0.08 mm. Both sides of the femoral condyle and the bottom of the tibial tray were fully constrained. Axial and anterior–posterior forces and rotational torques were applied to knee prostheses according to the international standard of ISO14243-1. Table 1 lists the material parameters of the tissue in the FE models.

Table 1 Material parameters

Material	Elastic modulus (GPa)	Poisson ratio
Bone	17	0.3
Cartilage	0.005	0.46
Meniscus	0.059	0.49
PEEK	3.5	0.4
UHMWPE	0.711	0.4

PEEK: polyether-ether-ketone; UHMWPE: ultrahigh molecular weight polyethylene

Statistical analysis

The experimental data were presented as mean±standard deviation. Statistical analysis was performed using SPSS software. Statistical significance was analyzed using the unpaired two-tailed Student's *t*-test. The *P*-values for the differences between groups were labeled as follows: $P>0.05$ (NS: not significant), $^{*}P<0.05$ (significant), $^{**}P<0.01$ (highly significant), and $^{***}P<0.001$ (extremely significant).

Results

Friction and wear properties

Figure 2 shows the tribological properties of PEEK pins with different printing orientations against UHMWPE plates. As shown in Fig. 2a, all the friction coefficient curves tended to be steady after 6000 cycles, indicating that they entered the stable period from the run-in period. Figure 2b provides the average friction coefficient. When the printing orientation of PEEK filaments was vertical to the sliding direction, the average friction coefficient was 0.23±0.05, which decreased to 0.14±0.03 (by 39.13%) at 0° orientation. Besides, while the friction coefficients of the friction pairs at 22.5° and 45° were not significantly different from that at 0°, there was a significant difference at 67.5° and 90°. As shown in Fig. 2c, the wear volumes of PEEK pins in all orientations were negative, indicating that instead of losing mass after wear, the mass of PEEK pins increased inversely. This might be due to the transfer of wear debris from UHMWPE to the surface of PEEK, which will be further discussed in the section about the microstructure. The total wear volume was considered when the PEEK and UHMWPE were regarded as a system

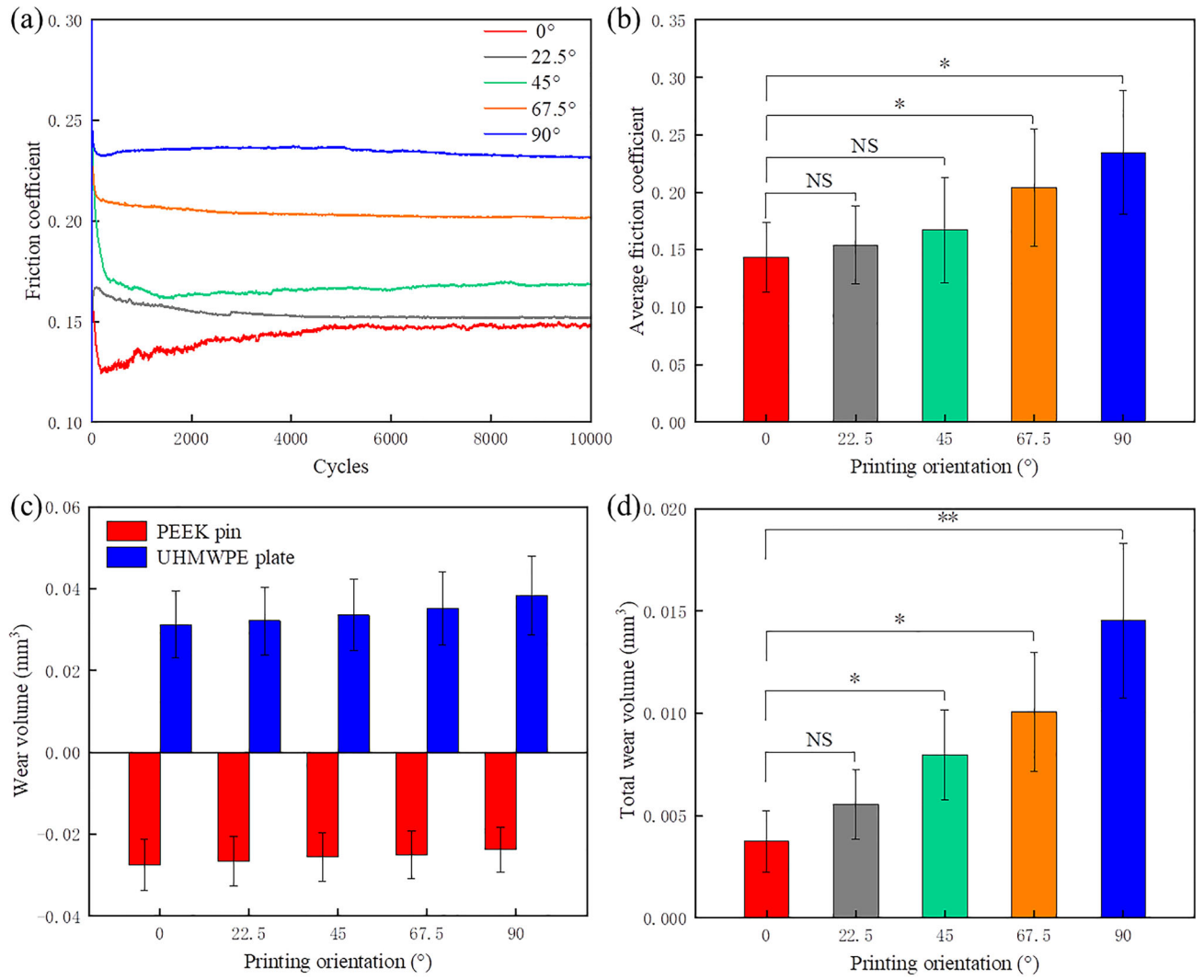

Fig. 2 Tribological properties of PEEK pins with different orientations against UHMWPE plates. **a** Friction coefficient curves. **b** Average friction coefficient. **c** Wear volume. **d** Total wear volume. Data are represented as mean±standard deviation, n=3. $^{*}P$<0.05, $^{**}P$<0.01. PEEK: polyether-ether-ketone; UHMWPE: ultrahigh molecular weight polyethylene; NS: not significant

(Fig. 2d). The total wear volume of friction pairs in different orientations was not zero, demonstrating that part of the wear debris flowed into the medium. The smaller the wear volume, the less the flow of wear debris into the medium. As the total wear volume at 0° was minimal compared to the other orientations, this orientation was considered optimal for the filaments in the 3D printing process.

As shown in Table 2, the wear rates of PEEK against UHMWPE were negative for all orientations, indicating that the volume of PEEK increased after friction. The wear rate decreased from $(-5.725\times10^{-6}\pm1.313\times10^{-6})$ mm^3/(N·m) at 0° orientation to $(-4.954\times10^{-6}\pm1.158\times10^{-6})$ mm^3/(N·m) at 90° orientation. However, the wear rates of UHMWPE were positive for all orientations, which implied a reduction in volume after wear. The wear rate increased from $(6.502\times10^{-6}\pm1.694\times10^{-6})$ mm^3/(N·m) at 0° orientation to $(7.981\times10^{-6}\pm1.983\times10^{-6})$ mm^3/(N·m) at 90° orientation. The total wear rate of friction pairs also showed a similar trend with the increased printing orientation, consistent with the wear volume (Figs. 2c and 2d).

Wear morphology

Figure 3 presents the microstructure of PEEK with different orientations after wear. White particles appeared on the surface of PEEK with different orientations at low magnifications (Figs. 3a1–3e1). At higher magnifications, these seemed to adhere to the surface of PEEK in an irregular and discontinuous sheet-like structure (Figs. 3a2–3e2). Based on the molecular chain characteristics of the couple materials,

Table 2 The wear rates of PEEK against UHMWPE

Printing orientation	Wear rate ($\times 10^{-6}$ $mm^3/(N \cdot m)$)		
	PEEK	UHMWPE	PEEK-UHMWPE
0°	−5.725±1.313	6.502±1.694	0.777±0.313
22.5°	−5.540±1.271	6.698±1.729	1.158±0.354
45°	−5.329±1.227	6.987±1.813	1.658±0.458
67.5°	−5.223±1.198	7.321±1.869	2.098±0.604
90°	−4.954±1.158	7.981±1.983	3.027±0.792

PEEK: polyether-ether-ketone; UHMWPE: ultrahigh molecular weight polyethylene

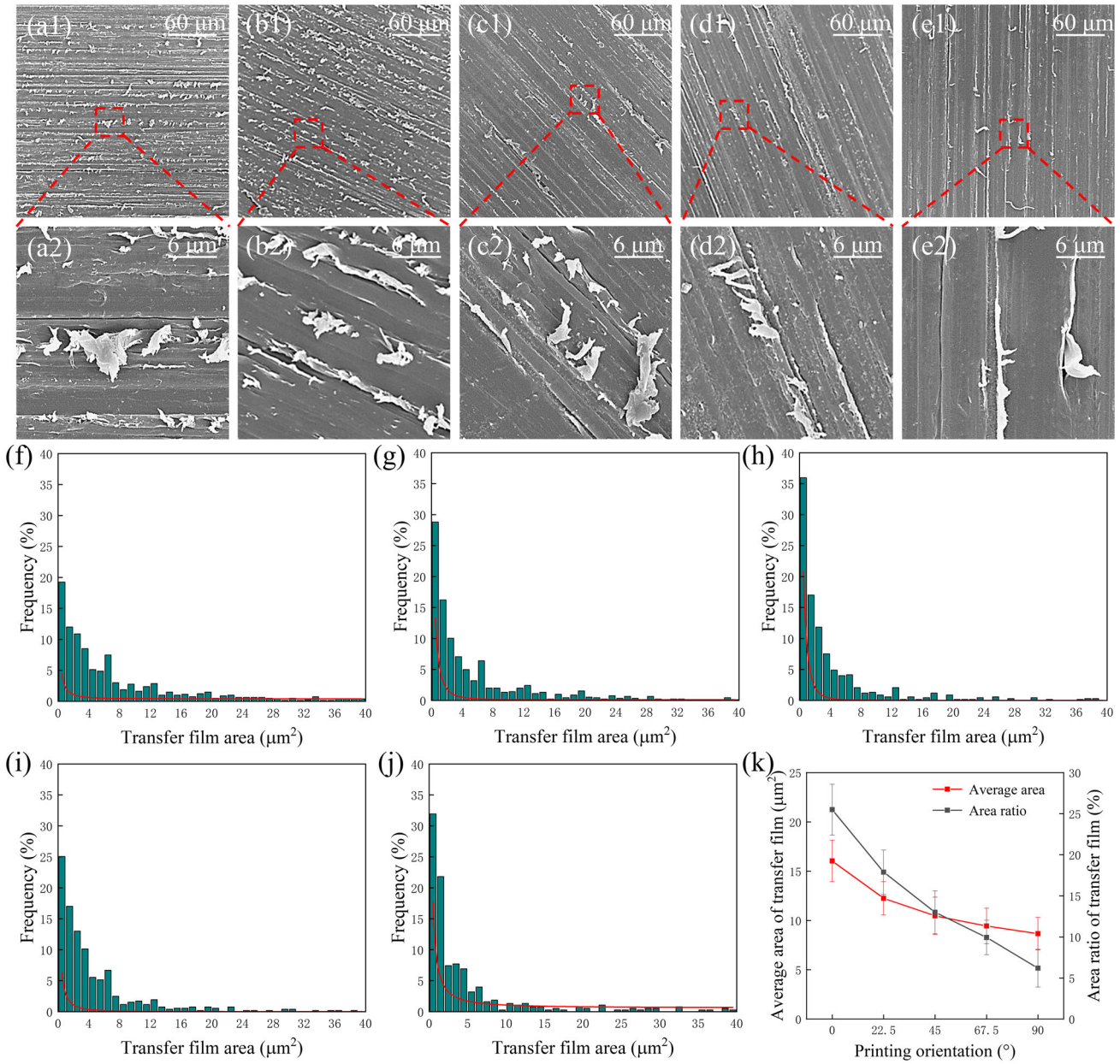

Fig. 3 Microstructure of PEEK with different orientations after friction at **a1**, **a2** 0°, **b1**, **b2** 22.5°, **c1**, **c2** 45°, **d1**, **d2** 67.5°, and **e1**, **e2** 90°. **f**–**j** Frequency distribution histograms of the transfer film area formed on the surfaces of PEEK at **f** 0°, **g** 22.5°, **h** 45°, **i** 67.5°, and **j** 90°. **k** Average area and area ratio of the transfer film (data are represented as mean±standard deviation, *n*=5). PEEK: polyether-ether-ketone

these countless tiny and isolated sheet-like structures were transfer films generated by the wear debris of UHMWPE. The transfer film was formed through material transference during the frictional process. The low-cohesion-density UHMWPE was conveyed onto the counterface surface of the high-cohesion-density PEEK, resulting in a thin film-like transitional layer between the contacting friction interfaces. The formation of transfer film was closely related to the microstructure and physicochemical properties of the materials and operating conditions, such as sliding velocity, load, environmental temperature, and humidity. Moreover, these influencing factors interacted with each other, creating a comprehensive frictional system. Interestingly, the characteristics of the transfer film formed on the surface of PEEK varied with the printing orientation. Regarding the number, more transfer films were formed on the surface of PEEK at low magnifications when the printing orientation of filaments was parallel to the sliding direction of wear. The number of transfer films decreased significantly when the orientation was changed from 0° to 90° as only a thin layer of transfer film could be observed on the surface of PEEK at 90°. In terms of size, the transfer film on the surface of PEEK at 0° was also larger than that at other orientations at high magnifications. Therefore, both the number and size of the transfer film formed on the surface of PEEK at 0° were higher than those at other orientations. Figures 3f–3k show the frequency distribution and ratio of the transfer film area. The average size and area ratio of the transfer film formed on PEEK with 0° orientation were (16.037±2.105) μm^2 and 25.49%, respectively, which decreased to (8.666±1.650) μm^2 and 6.2% at 90° orientation.

We analyzed the surface morphology of PEEK before and after friction at 0° orientation to understand the formation of the transfer film. As shown in Figs. 4a1–4a4, the surface of PEEK before friction showed a regularly arranged groove structure formed under the synergistic action of the regularly arranged PEEK filaments during the 3D printing and the subsequent polishing process. This groove structure could be considered a type of texture [36, 37]. At low magnifications, PEEK's surface appeared to have abundant isolated transfer films against UHMWPE, which were evenly distributed and linearly arranged along the edges of the grooves (Figs. 4b1 and 4b2). At high magnifications, the UHMWPE transfer film was found to be firmly bound to the PEEK matrix without large gaps (Figs. 4b3 and 4b4). Moreover, the extension direction of the transfer film was consistent with the sliding direction of friction. Using phase characterization, we demonstrated the formation of UHMWPE transfer films. First, XPS was used to quantitatively analyze the surface functional groups after wear. Both the control and test PEEK exhibited an O1s peak at 532.8 eV and a C1s peak at 284.5 eV (Fig. 4c). The C1s core level spectra of the control PEEK demonstrated C–C (284.8 eV) and C=O (288.5 eV) bonds (Fig. 4d). Particularly, a new peak appeared at 286.4 eV in the C1s core level spectra of the test PEEK (Fig. 4e), which corresponded to the C–O bond of UHMWPE [38, 39]. This process further substantiated the presence of UHMWPE transfer films on the surface of PEEK. Then, XRD of the phase change of the friction pair (Fig. 4f) showed that the virgin PEEK and UHMWPE exhibited characteristic diffraction peaks at 2θ=18.6°, 22.2°, 28.6°, 21.6°, and 24.1°. After friction, the characteristic diffraction peaks of UHMWPE remained unchanged, while a new characteristic diffraction peak of UHMWPE appeared at 2θ=24.1° in the inset of the PEEK spectrum. Based on the FTIR spectrum, the change in the functional groups of the friction pair was identified (Fig. 4g). Before and after friction, UHMWPE exhibited characteristic peaks of $–CH_2$ at 2914 cm^{-1} and 2846 cm^{-1}. However, PEEK also exhibited similar characteristic peaks as those of the $–CH_2$ of UHMWPE after friction, which indicated that UHMWPE debris was transferred onto the surface of PEEK. This further certified that the sheet-like structure on the surface of PEEK was UHMWPE, which adhered to the surface of PEEK to form the transfer film.

The printing orientation of PEEK filaments during 3D printing significantly impacts the morphology of UHMWPE after wear. The surface of UHMWPE at 0° orientation formed light and thin furrows with an average width of (22.8±4.3) μm (Fig. 5a), whose boundaries are represented by the two red lines. As shown in Fig. 5b, the width of these furrows increased to (45.5±6.1) μm at 22.5° orientation, making their boundaries more distinct, and further increased to (106.3±10.9) μm at 45° orientation (Fig. 5c). In addition to the increase in the furrow width to (132.6±18.4) μm at 67.5° orientation (Fig. 5d), the surface had also developed numerous minute abrasions, although they were not readily apparent. The furrow width was the highest at 90°, which was (197.5±27.1) μm. Furthermore, we observed distinct boundaries between each furrow (Fig. 5e). Figures 5f–5j show the visual 3D morphology of UHMWPE. The surface of UHMWPE was flat at 0° orientation, while numerous wide and deep furrows appeared on the surface with the increased orientation. While the corresponding wear depth curve of UHMWPE was steady at 0° orientation, it started to fluctuate drastically from 45° to 90° orientations, which highlighted that the printing orientation of the PEEK pins significantly influenced the wear of the UHMWPE plate. The wear morphology of UHMWPE was further analyzed quantitatively by Ra and the wear depth (Fig. 5k). Ra of UHMWPE at 0° was (0.559±0.194) μm, which increased to (3.179±0.410) μm at 90°, showing a significant difference. Similarly, the wear depth of UHMWPE against PEEK at 0° exhibited a significant difference compared to that at 45°, 67.5°, and 90° orientations. The results of the quantitative analysis confirmed that the least wear was obtained when the printing

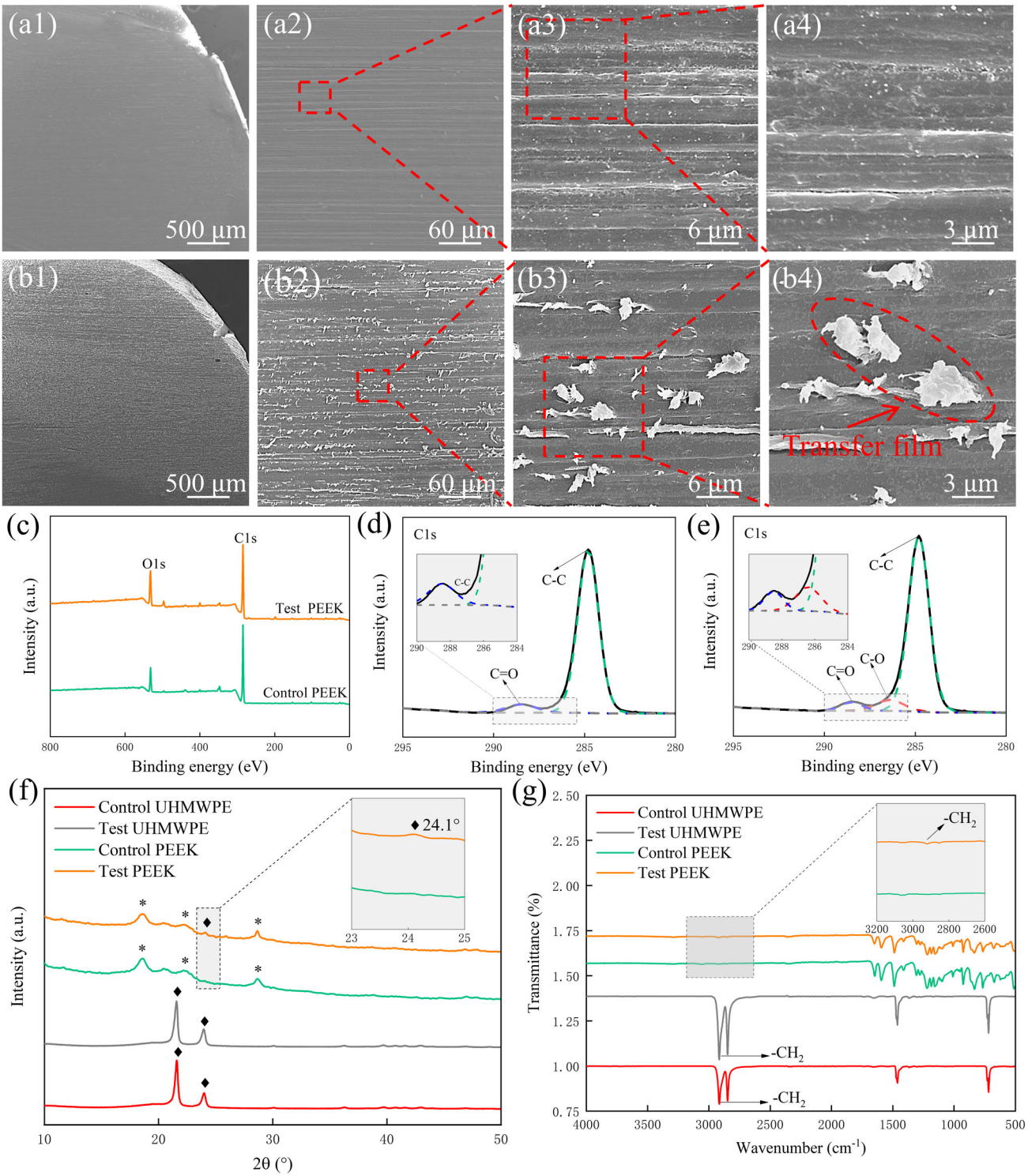

Fig. 4 Characteristics of the transfer film. SEM images of PEEK **a1**–**a4** before and **b1**–**b4** after friction. **c** XPS spectra of PEEK. C1s core level spectra of **d** control and **e** test PEEK. **f** XRD spectra. **g** FTIR patterns. SEM: scanning electron microscopy; PEEK: polyether-ether-ketone; XPS: X-ray photoelectron spectroscopy; XRD: X-ray diffractometer; FTIR: Fourier transform infrared spectroscopy; UHMWPE: ultrahigh molecular weight polyethylene

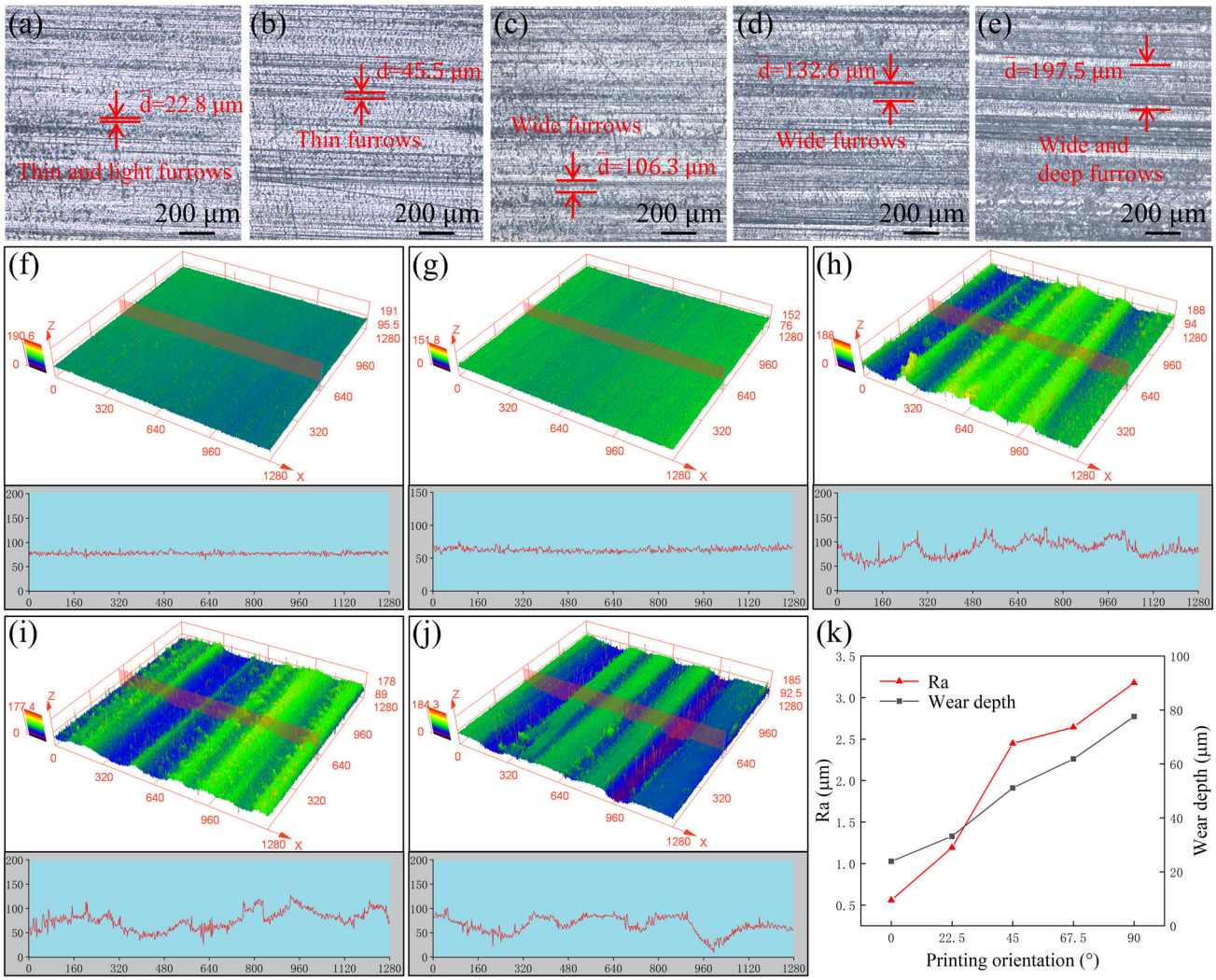

Fig. 5 Characterization of UHMWPE morphologies. 2D morphologies of UHMWPE against PEEK at **a** 0°, **b** 22.5°, **c** 45°, **d** 67.5°, and **e** 90°. 3D morphologies of UHMWPE against PEEK at **f** 0°, **g** 22.5°, **h** 45°, **i** 67.5°, and **j** 90°. **k** Ra and wear depth. UHMWPE: ultrahigh molecular weight polyethylene; PEEK: polyether-ether-ketone; Ra: surface roughness

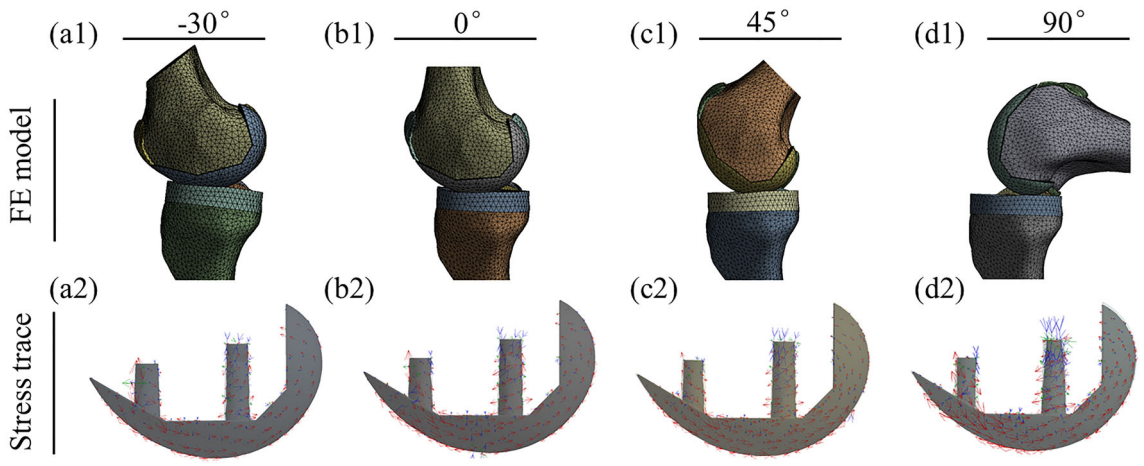

Fig. 6 Finite element (FE) analysis of knee joint under different flexion angles. **a1–d1** FE models. **a2–d2** Stress traces

orientation of filaments was parallel to the sliding direction of friction.

Application of the printing orientation in the design of knee prosthesis

Based on the frictional experiments, the tribological properties were considered the best when the printing orientation of filaments was parallel to the sliding direction of friction. This can be used to design the printing path of a joint prosthesis. Moreover, the stress trace can clearly display the stress distribution of joint prostheses, providing a criterion for designing the 3D printing path. Therefore, the FE models of knee prosthesis were constructed at −30°, 0°, 45°, and 90° flexion angles (Figs. 6a1–6d1), and the corresponding stress traces were presented in Figs. 6a2–6d2. The stress traces of the exterior were found to be distributed along the profile of the femoral condyle at different angles (shown with a red arrow), indicating that the exterior was mainly subjected to shear stress. Moreover, the stress traces of the inner were diverse in different directions: vertical to horizontal plane at 0° and the rear plane at 90° direction. This suggests that the stress traces mainly subjected to compressive stress might change with the motor direction. Besides, the two fixed columns were mainly subjected to common stress in the vertical and horizontal directions. The stress trace can clearly display the stress distribution of the knee femoral condyle under external load, providing a criterion for designing the joint prosthesis printing path.

The stress traces at different flexion angles were integrated to form the overall stress trace diagram (Fig. 7a). In addition to the anteroposterior force and rotational torque (indicated by the thin black arrows), the knee femoral condyle was primarily subjected to axial forces (indicated by the thick black arrows). Besides, the design of the printing path also needs to consider the motorial direction of the knee joint. The knee joint primarily displays "rolling" movement from straight to flexion of 20° and "sliding" from 20° to full flexion (Fig. 7b). Based on the above criteria, the concrete printing paths of different regions are shown in Fig. 7c. According to the distribution of the stress traces on the exterior of the femoral condyle along the external profile, the exterior was designed as a concentric path to reduce the friction coefficient and improve the wear resistance performance. As the stress traces on the interlayer of the femoral condyle change at different flexion angles, the interlayer was divided into four regions, and each region was designed as a straight path perpendicular to the respective inner surface to enhance the overall mechanical properties. The inner was designed as a porous path with several layers to promote the bonding strength between the knee femoral condyle prosthesis and bone tissue.

The slice model of the femoral condyle was placed in a lateral position for printing with the long axes of fixation columns parallel to the printing base (Fig. 8a). The knee prosthesis was successfully fabricated via an FFF 3D process according to the pre-designed printing paths. As shown in Fig. 8b, the exterior surface of the PEEK femoral condyle was smooth with a surface roughness of (1.508±0.217) μm; the inner possessed a 3D interconnected porous structure with a pore size of (800±42) μm. This example will enable the development of 3D-printed knee prostheses, which might benefit patients requiring multifunctional knee joint replacements in the future.

Discussion

Although artificial joint prostheses are currently prepared using an injection molding process, they are limited by complex shape structure, expensive mold development, and long preparation cycles. Due to the increased demand for joint prostheses with improved therapeutic effects, personalized joint prostheses must be developed. Three-dimensional printing can directly build personalized appearance structures in a short time by stacking materials layer by layer, providing a personalized and economical solution.

The unique printing orientation during the 3D printing of PEEK determines its tribological properties. The friction coefficient and wear rate of the friction pair were 0.14±0.03 and $(0.777\times10^{-6}\pm0.313\times10^{-6})$ $mm^3/(N\cdot m)$ (Fig. 2), slightly higher than those of the injection molded friction pair [21], which might be due to several reasons. First, the 3D-printed PEEK and UHMWPE friction pair underwent only 10,000 cycles before entering the stable friction period, while other studies that reported lower wear rates had longer test durations [22]. This study aims to obtain the optimal printing orientation of tribological property to achieve the reasonable distribution of the printing path on the prosthesis. Therefore, considering the research purpose and time cost, this test was performed using a short cycle. Second, in a previous study, the wear volume was removed in the run-in and severe wear periods, and the wear rate was only calculated in the stable period, resulting in lower wear rates than in this study [19].

The formation of the UHMWPE transfer film on the surface of PEEK was discussed. In the initial stage of friction, the micro bulges on the surface of PEEK were embedded in the interior of UHMWPE due to higher hardness. They cut off the surface material of UHMWPE to form wear debris during sliding. Afterward, this wear debris would be mechanically captured by the hills and valleys of the groove texture of PEEK and temporarily stored in the valleys. Finally, the UHMWPE wear debris gradually adhered to the surface of PEEK to form a transfer film under the reduplicative action of contact stress. The hills' stress of groove texture was too high for wear debris to enter, and the valleys' stress was too

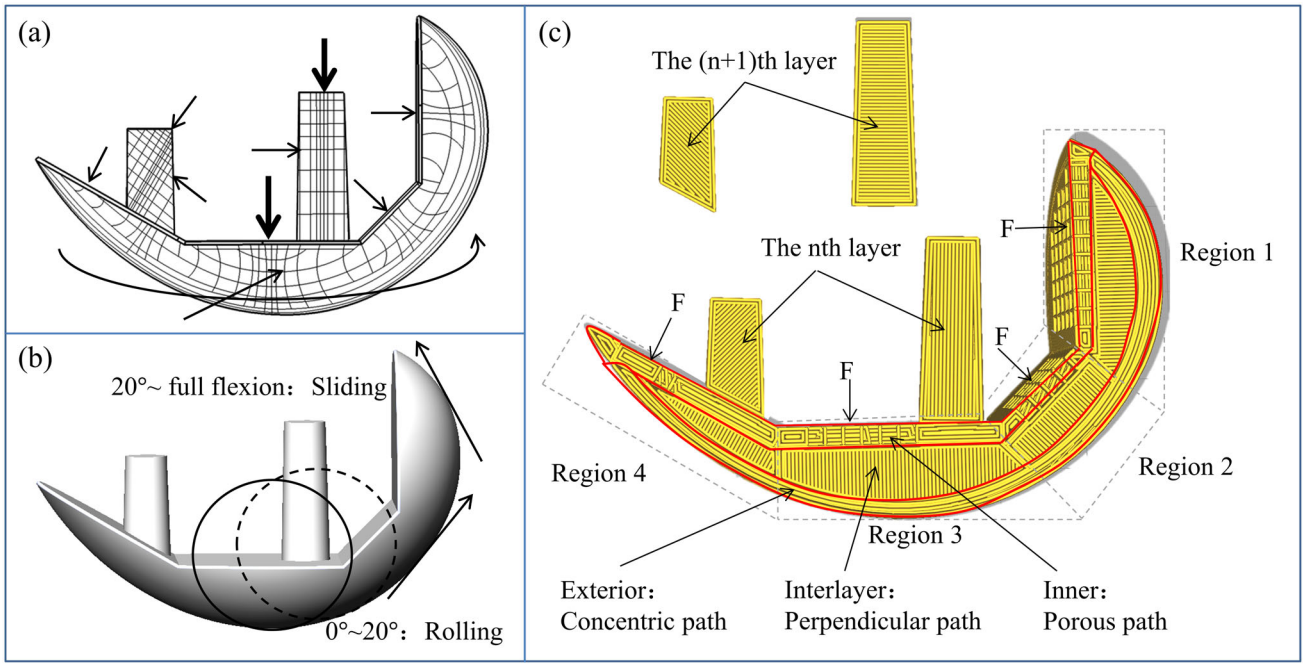

Fig. 7 Application of printing orientation in the design of the knee prostheses. **a** Stress traces. **b** Movement forms of the knee joint. **c** Design of 3D printing path

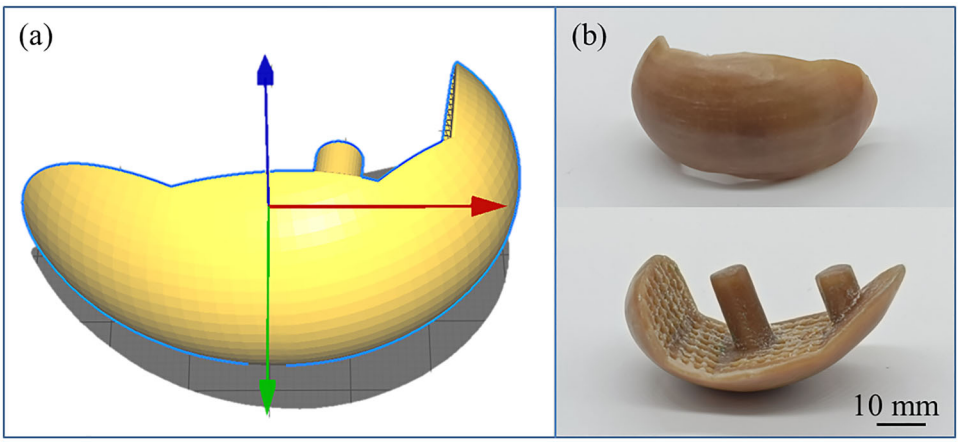

Fig. 8 Knee prosthesis. **a** Placing form of the model and **b** PEEK femoral condyle prosthesis. PEEK: polyether-ether-ketone

low for wear debris to adhere on the surface of PEEK, so the transfer film mainly followed the transition area between the hills and valleys, namely the edge distribution of the groove texture (Figs. 3 and 4).

We also analyzed the effect of the printing orientation on the transfer film's characteristics. The contact stress of the wear debris on the hills of the groove texture was much greater than that in the valleys during friction. When the printing orientation of the PEEK filaments was parallel to the sliding direction, the wear debris could continuously slide along the hills and valleys of the groove texture (Fig. 9). Resultantly, the transfer film formed at 0° orientation was larger both in number and size (Figs. 3a1 and 3a2). However, when the printing orientation of the PEEK filaments was perpendicular to the sliding direction, the wear debris alternately makes contact with the hills and valleys between groove textures. Consequently, the corresponding contact stress changes from the minimum in the valleys to the maximum in the hills and then is repeated intermittently. This is not conducive to forming a firm transfer film on the surface of PEEK, reducing the number and size of the transfer film at 90° orientation, as seen in Figs. 3e1 and 3e2. Therefore, steady stress is an important factor affecting the transfer film formation.

Although recent reports have shown the tribological behavior of PEEK, the surface did not appear to have a transfer film [19, 21, 22]. This might be due to the unique surface morphology formed by the 3D printing process. These PEEK

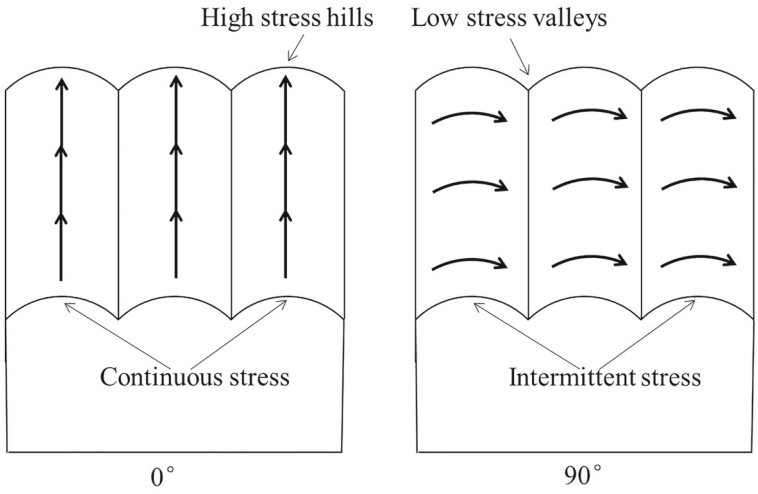

Fig. 9 Schematic of the effect of different printing orientations of PEEK on the transfer film formation. PEEK: polyether-ether-ketone

specimens were all fabricated by traditional injection molding process with a surface roughness of Ra<0.1 μm. As this smooth surface was not conducive to capturing and storing wear debris, the UHMWPE wear debris could not adhere to the surface of the injection molded PEEK to form a transfer film. The 3D printing surface of PEEK was formed by a regular arrangement of filaments, resulting in a groove texture (Fig. 4) that could mechanically capture wear debris to form a transfer film under the action of contact stress. The friction coefficient and wear rate were decreased with an increase in the transfer film formation (Fig. 2). In conclusion, 3D-printed PEEK possessed a unique advantage in the construction of groove morphology to form a transfer film that bridges PEEK and UHMWPE, altering the contact form between the friction pair. The transfer film enveloped sharp surface features, preventing direct frictional interaction between the hard PEEK and relatively soft UHMWPE, and resulting in lower friction coefficients and improved wear resistance.

Furthermore, the wear mechanism of PEEK against UHMWPE was analyzed. Several furrows appeared on the surface of UHMWPE, which changed from light and thin to deep and wide with the increasing orientation (Fig. 5). These furrows could be attributed to the microcutting effect of the PEEK groove texture on UHMWPE. As the sliding contact area between PEEK and UHMWPE was smaller at 0° orientation compared with other orientations, the microcutting effect was slight, imparting the best corresponding tribological properties. Based on the above analysis, the wear mechanism of 3D-printed PEEK against UHMWPE can be considered as "abrasive wear."

The wear debris flowing into the serum is harmful and can cause osteolysis [40, 41]. In this study, a part of the wear debris flowed into the serum, while the rest adhered to the surface of PEEK, forming a transfer film. This film can cover the matrix material of the friction pair to improve the tribological properties and reduce the flow of debris into the serum, preventing osteolysis [42, 43]. Further, although the PEEK pins were cleaned ultrasonically after the wear test, the microstructure analysis showed that the UHMWPE transfer film remained adhered to the surface of PEEK, even after the ultrasonic treatment (Figs. 3 and 4), indicating that the UHMWPE transfer film firmly adhered to PEEK. A strong bond between the transfer film and matrix might enhance the wear life of the transfer film and avoid its shedding into the serum, preventing biological damage.

Using an example, we demonstrated the potential benefits of considering printing orientation in the design of medical devices, such as knee prostheses. The complicated mechanical environment of the knee joint gave rise to complex stress changes in the femoral condyle. Therefore, the 3D printing path of the prostheses should be designed in combination with the functional requirements of different regions. In a knee prosthesis, the exterior of the femoral condyle rubs against the tibial tray for several years or even longer. Therefore, the exterior of the femoral condyle of an ideal knee prosthesis should possess excellent wear resistance, and the inner should support the growth of the bone tissue into the femoral condyle to achieve biological fixation between the prosthesis and bone tissue for adequate biological activity. Besides, the knee prosthesis must also have sufficient mechanical strength to withstand external loads. When the exterior of the femoral condyle is designed in a concentric path, a consistent movement direction can be maintained with the printing orientation of PEEK filaments regardless of rolling or sliding, resulting in excellent wear resistance of the exterior. Due to the anisotropy of the mechanical properties via 3D printing, and under the premise of the external concentric path, the straight path of the interlayer could ensure optimal mechanical strength. Overall, this example highlighted the potential of 3D printing orientation to improve the performance and functionality of joint prostheses.

Conclusions

In summary, we fabricated PEEK pins using FFF 3D printing, and investigated the effects of the printing orientation on the tribological properties of PEEK using a pin-on-plate tribometer in 25% newborn calf serum. Based on the friction and wear tests, we made the following conclusions.

(1) A transfer film formed on the surface of PEEK against UHMWPE can be attributed to the groove morphology generated by the regular arrangement of PEEK filaments, which mechanically captures the wear debris.
(2) The size and number of transfer films depended on the printing orientation of PEEK. When the printing orientation was parallel to the sliding direction of friction, the transfer film was larger than it was with other orientations due to more continuous stress, which is conducive to the adhesion of wear debris to the surface of PEEK.
(3) The transfer film between PEEK and UHMWPE improved the tribological properties of the friction pair by covering the matrix materials. Resultantly, the friction coefficient and wear rate were significantly reduced, by 39.13% and 74.33%, respectively.
(4) We presented a new perspective for the printing orientation of PEEK in the design of knee prostheses to facilitate the development of 3D-printed artificial joints. The optimal printing orientation endowed the knee prosthesis with excellent friction resistance and mechanical and biological properties.

Acknowledgements This study was supported by the following funds: (1) National Key R&D Program of China (No. 2018YFE0207900); (2) Program for Innovation Team of Shaanxi Province (No. 2023-CX-TD-17); (3) Program of the National Natural Science Foundation of China (No. 51835010); (4) Key R&D Program of Guangdong Province (No. 2018B090906001); (5) Natural Science Basic Research Program of Shaanxi Province (No. 2022JQ-378); (6) China Postdoctoral Science Foundation (No. 2020M683458); (7) Fundamental Research Funds for the Central Universities; (8) Youth Innovation Team of Shaanxi Universities.

Author contributions YL contributed to conceptualization, methodology, data curation and writing-original draft; JBZ contributed to conceptualization, methodology and investigation; CNS contributed to conceptualization, validation and formal analysis; DCL contributed to funding acquisition and administration, and reviewed the initial versions of the manuscript. All authors have read and approved the final manuscript.

Declarations

Conflict of interest The authors declare that they have no conflict of interest.

Ethical approval This article does not contain any studies with human or animal subjects performed by any of the authors.

Data availability The data used to support the findings of this study are available from the corresponding author upon request.

References

1. Gullbrand SE, Ashinsky B, Bonnevie ED (2018) Long-term mechanical function and integration of an implanted tissue-engineered intervertebral disc. Transl Med Sci 10(468):eaau0670. https://doi.org/10.1126/scitranslmed.aau0670
2. Yang ML, Yang LY, Peng SP et al (2023) Laser additive manufacturing of zinc: formation quality, texture, and cell behavior. Bio-Des Manuf 6(2):103–120. https://doi.org/10.1007/s42242-022-00216-0
3. Zhang A, Chen H, Liu Y et al (2021) Customized reconstructive prosthesis design based on topological optimization to treat severe proximal tibia defect. Bio-Des Manuf 4(1):87–99. https://doi.org/10.1007/s42242-020-00102-7
4. Cheng KY, Gopal V, Mcnallan M et al (2019) Enhanced tribocorrosion resistance of hard ceramic coated Ti–6Al–4V alloy for hip implant application: in-vitro simulation study. Acs Biomater Sci Eng 5(9):4817–4824. https://doi.org/10.1021/acsbiomaterials.9b00609
5. Bandyopadhyay A, Shivaram A, Isik M (2019) Additively manufactured calcium phosphate reinforced CoCrMo alloy: biotribological and biocompatibility evaluation for load-bearing implants. Addit Manuf 28:312–324. https://doi.org/10.1016/j.addma.2019.04.020
6. Xu HD, Zhang DK, Chen K (2019) Taper fretting behavior of PEEK artificial hip joint. Tribol Int 137:30–38. https://doi.org/10.1016/j.triboint.2019.04.027
7. Han XT, Sharma N, Xu ZQ et al (2019) An in vitro study of osteoblast response on fused-filament fabrication 3D printed PEEK for dental and cranio-maxillofacial implants. J Clin Med 8(6):771. https://doi.org/10.3390/jcm8060771
8. Liu G, Zhang LG, Li GT et al (2019) Tuning the tribofilm nanostructures of polymer-on-metal joint replacements for simultaneously enhancing anti-wear performance and corrosion resistance. Acta Biomater 87:285–295. https://doi.org/10.1016/j.actbio.2019.01.038
9. Oladapo BI, Zahedi SA, Ismail SO et al (2021) 3D printing of PEEK–cHAp scaffold for medical bone implant. Bio-Des Manuf 4(1):44–59. https://doi.org/10.1007/s42242-020-00098-0
10. Lin ZB, Yue HQ, Gao BZ (2020) Enhancing tribological characteristics of PEEK by using PTFE composite as a sacrificial tribofilm-generating part in a novel dual-pins-on-disk tribometer. Wear 460–461:203472. https://doi.org/10.1016/j.wear.2020.203472
11. Zhang YH, Wei T, Yu Z et al (2018) Continuous carbon fiber/crosslinkable poly(ether ether ketone) laminated composites with outstanding mechanical properties, robust solvent resistance and excellent thermal stability. Compos Sci Technol 165:148–153. https://doi.org/10.1016/j.compscitech.2018.06.020
12. Li YD, Jia H, Cui XH et al (2022) Bending properties, compression properties, biocompatibility and bioactivity of sulfonated carbon fibers/PEEK composites with graphene oxide coating. Appl Surf Sci 575:151774. https://doi.org/10.1016/j.apsusc.2021.151774
13. Zheng JB, Zhao HY, Dong EC et al (2021) Additively-manufactured PEEK/HA porous scaffolds with highly-controllable mechanical properties and excellent biocompatibility. Sci Eng C Mater Biol Appl 128:112333. https://doi.org/10.1016/j.msec.2021.112333
14. Feng S, Liu C, Sue HJ (2022) Preparation of PEEK/MWCNT nanocomposites via MWCNT-induced interfacial crystallization

mediated compatibilization. Compos Sci Technol 221:109298. https://doi.org/10.1016/j.compscitech.2022.109298
15. Wang ZQ, Ni J, Gao DR (2018) Combined effect of the use of carbon fiber and seawater and the molecular structure on the tribological behavior of polymer materials. Friction 6(2):183–194. https://doi.org/10.1007/s40544-017-0164-8
16. Chamberlain KA, Rankin KS, Briscoe A et al (2017) Wear properties of poly-ether-ether-ketone bearing combinations under zero and cross shear kinematics in total knee arthroplasty. J Biomed Mater Res B 107(2):445–453. https://doi.org/10.1002/JBM.B.34136
17. Liang YN, Gao DR, Zhao JH (2020) Tribological properties of friction pair between 316L stainless steel and CF/PEEK with nonsmooth surface under seawater lubrication. Tribol Trans 63(4):658–671. https://doi.org/10.1080/10402004.2020.1734704
18. Kandemir G, Smith S, Joyce TJ (2019) Wear behaviour of CFR PEEK articulated against CoCr under varying contact stresses: low wear of CFR PEEK negated by wear of the CoCr counterface. J Mech Behav Biomed 97:117–125. https://doi.org/10.1016/j.jmbbm.2019.05.022
19. East RH, Briscoe A, Unsworth A (2015) Wear of PEEK-OPTIMA® and PEEK-OPTIMA®-wear performance articulating against highly cross-linked polyethylene. Proc Inst Mech Eng Part H J Eng Med 229(3):187–193. https://doi.org/10.1177/0954411915576353
20. Scholes SC, Unsworth A (2019) Wear studies on the likely performance of CFR-PEEK/CoCrMo for use as artificial joint bearing materials. J Mater Sci Mater Med 20(1):163–170. https://doi.org/10.1007/s10856-008-3558-3
21. Cowie RM, Pallem NM, Jennings LM et al (2020) Third body wear of UHMWPE-on-PEEK-OPTIMA™. Materials 13(6):1264. https://doi.org/10.3390/ma13061264
22. Cowie RM, Briscoe A, Fisher J et al (2019) Wear and friction of UHMWPE-on-PEEK OPTIMA™. J Mech Behav Biomed 89:65–71. https://doi.org/10.1016/j.jmbbm.2018.09.021
23. Brockett CL, Carbone S, Fisher J et al (2017) PEEK and CFR-PEEK as alternative bearing materials to UHMWPE in a fixed bearing total knee replacement: an experimental wear study. Wear 374–375:86–91. https://doi.org/10.1016/j.wear.2016.12.010
24. Cowie RM, Briscoe A, Fisher J et al (2016) PEEK-OPTIMA™ as an alternative to cobalt chrome in the femoral component of total knee replacement: a preliminary study. Proc Inst Mech Eng Part H J Eng Med 230(11):1008–1015. https://doi.org/10.1177/0954411916667410
25. Zhang T, Liu HT, Zhang DK et al (2019) Mechanical and wear properties of polyetheretherketone composites filled with basalt fibres. Sci Eng Compos Mater 26(4):317–326. https://doi.org/10.1515/secm-2019-0016
26. Li Z, Haddouti E, Welle K et al (2020) The effects of biomaterial implant wear debris on osteoblasts. Front Cell Dev Biol 8:352. https://doi.org/10.3389/fcell.2020.00352
27. Yan Z, Tian XX, Zhu JY et al (2018) Metformin suppresses UHMWPE particle-induced osteolysis in the mouse calvaria by promoting polarization of macrophages to an anti-inflammatory phenotype. Mol Med 24(1):20. https://doi.org/10.1186/s10020-018-0013-x
28. Yuan T, Terkawi MA, Onodera T et al (2020) Blockade of XCL1/lymphotactin ameliorates severity of periprosthetic osteolysis triggered by polyethylene-particles. Front Immunol 11:1720. https://doi.org/10.3389/fimmu.2020.01720
29. Rafiee M, Farahani R, Therriault D (2020) Multi-material 3D and 4D printing: a survey. Adv Sci 7(12):1902307. https://doi.org/10.1002/advs.201902307
30. Kim JY, Kim WJ, Kim GH (2020) Scaffold with micro/nanoscale topographical cues fabricated using E-field-assisted 3D printing combined with plasma-etching for enhancing myoblast alignment and differentiation. Appl Surf Sci 509:145404. https://doi.org/10.1016/j.apsusc.2020.145404
31. Redondo E, Pumera M (2021) Fully metallic copper 3D-printed electrodes via sintering for electrocatalytic biosensing. Appl Mater Today 25:101253. https://doi.org/10.1016/j.apmt.2021.101253
32. Basgul C, Thieringer FM, Kurtz SM (2021) Heat transfer-based non-isothermal healing model for the interfacial bonding strength of fused filament fabricated polyetheretherketone. Addit Manuf 46:102097. https://doi.org/10.1016/j.addma.2021.102097
33. Doyle SE, Snow F, Duchi S (2021) 3D printed multiphasic scaffolds for osteochondral repair: challenges and opportunities. Int J Mol Sci 22(22):12420. https://doi.org/10.3390/ijms222212420
34. Zhiani Hervan S, Altnkaynak A, Parlar Z (2021) Hardness, friction and wear characteristics of 3D-printed PLA polymer. Proc Inst Mech Eng Part J J Eng Tribol 235(8):1590–1598. https://doi.org/10.1177/1350650120966407
35. Aziz R, UI Haq MI, Raina A (2020) Effect of surface texturing on friction behaviour of 3D printed polylactic acid (PLA). Polym Test 85:106434. https://doi.org/10.1016/j.polymertesting.2020.106434
36. Luo M, Huang SY, Man ZY et al (2022) Tribological behaviour of fused deposition modelling printed short carbon fibre reinforced nylon composites with surface textures under dry and water lubricated conditions. Friction 10(12):2045–2058. https://doi.org/10.1007/s40544-021-0574-5
37. Shang QB, Yu AB, Wu JZ et al (2017) Influence of heat affected zone on tribological properties of CuSn6 bronze laser dimple textured surface. Tribol Int 105:158–165. https://doi.org/10.1016/j.triboint.2016.10.008
38. Li WW, Meng L, Wang L et al (2016) Surface modification of ultra-high molecular weight polyethylene fibers by chromic acid. Surf Interface Anal 48(12):1316–1319. https://doi.org/10.1002/sia.6040
39. Zhu L, Dikin DA, Percec S et al (2021) Improving interlayer adhesion of poly(p-phenylene terephthalamide)(PPTA)/ultra-high-molecular-weight polyethylene (UHMWPE) laminates prepared by plasma treatment and hot pressing technique. Polymers 13(16):2600. https://doi.org/10.3390/polym13162600
40. Klapperich C, Graham J, Pruitt L et al (1999) Failure of a metal-on-metal total hip arthroplasty from progressive osteolysis. J Arthroplast 14(7):877–881. https://doi.org/10.1016/S0883-5403(99)90042-6
41. Murali R, Frcpa M, Bonar F et al (2008) Osteolysis in third-generation alumina ceramic-on-ceramic hip bearings with severe impingement and titanium metallosis. J Arthroplast 23(8):13–19. https://doi.org/10.1016/j.arth.2007.10.020
42. Sarraf M, Rezvani Ghomi E, Alipour S et al (2022) A state-of-the-art review of the fabrication and characteristics of titanium and its alloys for biomedical applications. Bio-Des Manuf 5(2):371–395. https://doi.org/10.1007/s42242-021-00170-3
43. Eger M, Hiram-Bab S, Liron T et al (2018) Mechanism and prevention of titanium particle-induced inflammation and osteolysis. Front Immunol 9:2963. https://doi.org/10.3389/fimmu.2018.02963